Proceedings of Symposia in Applied Mathematics

An Introduction to X-ray tomography and Radon Transforms

Eric Todd Quinto

Abstract. This article provides an introduction to the mathematics behind X-ray tomography. After explaining the mathematical model, we will consider some of the fundamental theoretical ideas in the field, including the projection slice theorem, range theorem, inversion formula, and microlocal properties of the underlying Radon transform. We will use this microlocal analysis to predict which singularities of objects will be well reconstructed from limited tomographic data. We will introduce specific limited data problems: the exterior problem, region of interest tomography, and limited angle region of interest tomography, and we use some of the author's reconstructions for these problems to illustrate the microlocal predictions about singularities. The appendix includes proofs of the basic microlocal properties of the Radon transform. Our overarching goal is to show some of the ways integral geometry and microlocal analysis can help one understand limited data tomography.

1. Introduction

The goal of tomography is to recover the interior structure of a body using external measurements, and tomography is based on deep pure mathematics and numerical analysis as well as physics and engineering. In this article, we will introduce some of the fundamental mathematical concepts in X-ray tomography and microlocal analysis and apply them to limited data problems. In the process, we will outline how the problems come up in practice and show what the microlocal

2000 *Mathematics Subject Classification.* Primary: 92C55, 44A12 Secondary: 35S30, 58J40.

Key words and phrases. Tomography, Radon Transform, Microlocal Analysis.

I am indebted to many researchers including, but not limited to the following people. Allan Cormack was a mentor to me, and he introduced me to the field of tomography and the exterior problem (§3.1). Allan and I enjoyed solving pure mathematical problems, too. Carlos Berenstein, Larry Shepp, and Larry Zalcman helped me as I began my career. Frank Natterer and Alfred Louis have been invaluable as I learned more, showing how deep analysis and numerical work go hand in hand. I learned about and appreciated Lambda CT from Kennan Smith and Adel Faridani. Victor Guillemin and Sig Helgason gave me a love of microlocal analysis and integral geometry. Peter Kuchment provided very helpful comments on material that appeared in a related article [**38**], and Matthias Hahn and Gestur Ólafsson corrected some misprints. I thank these folks, the other speakers in this short course, and other friends for making it all fun. This research is based upon work supported by the National Science Foundation under grants DMS-0200788 and DMS-0456858 and Tufts University FRAC.

analysis says for these problems. This is not a survey of the various types of tomography, rather a more detailed look at X-ray tomography and the mathematics behind it. For more information, we refer the reader to the other articles in this proceedings as well as sources such as [**18, 26, 73, 75, 27, 32, 52, 53, 11, 38, 59**] for details and further references on tomography and related problems in integral geometry.

We will start by explaining the mathematical model of X-ray tomography (§2). Then we will prove some of the basic theorems in the field. In section 2.2 we describe the microlocal properties of the Radon transform. In Section 3 we introduce the limited data problems and explain the challenges of limited data reconstruction, illustrating them with some of the author's reconstructions. Finally, in the appendix we provide proofs of the microlocal properties of the Radon transform.

2. X-ray Tomography

The goal of X-ray computed tomography (CT) is to get a picture of the internal structure of an object by X-raying the object from many different directions. We consider this problem in the plane and Alfred Louis will discuss the three-dimensional case [**44**].

As X-rays travel on a line L from the X-ray source through the object to an X-ray detector, they are attenuated by the material on the line L (we will neglect scatter and diffraction). According to Beer's law, the X-rays at a point x are attenuated proportionally to the number there, and the proportionality constant is called the *linear attenuation coefficient*. If the X-rays are monochromatic, then the linear attenuation coefficient is proportional to the density of the object; we will assume units are chosen so that the attenuation coefficient is equal to the density[1]. So, let $f : \mathbb{R}^2 \to \mathbb{R}$ be the density of the object. Mathematically, the goal of X-ray CT is to recover f from these measurements. Thus, according to Beer's Law, if $I(x)$ is the number of X-ray photons in the beam when it arrives at x, then the intensity in a small segment of length Δx is decreased by the multiplicative factor $f(x)\Delta x$, so:

$$\Delta I \approx -\big(f(x)\Delta x\big)I(x)\,. \tag{2.1}$$

By separating variables and integrating (2.1) from the source to the detector, we get the following integral transform:

$$\ln\left[\frac{I(\text{source})}{I(\text{detector})}\right] = \int_L f(x)\,dx_L =: Rf(L).$$

This integral transform R is exactly the classical Radon transform of f on the line L [**27, 52**], and since $I(\text{source})$ and $I(\text{detector})$ are measured, the line integral $Rf(L)$ is known.

Remarkably, Radon invented this transform in 1917 for pure mathematical reasons [**69**]. Apparently, Lorentz had previously developed the transform in $\mathbb{R}^3$, but he never published it [**27**, p. 51]. It wasn't until Allan Cormack reinvented it in 1963 [**7, 8**] that it was used in tomography. Cormack won the Nobel Prize in Medicine in 1979 because he proposed using this transform to reconstruct the density of the

[1]If the X-rays are not monochromatic, then lower energy X-rays get attenuated more than higher energy X-rays, so the average energy of X-rays increases as they go through the object. This is called *beam-hardening*, and it can create reconstruction artifacts (e.g., [**75**]).

body from X-ray images from different directions; he gave a mathematical formula to do the reconstruction; and he implemented his ideas by building and testing a prototype CT scanner. Godfrey Hounsfield shared the prize for his independent work deriving an algorithm and making a medical CT scanner.

Complete tomographic data are X-ray data over all lines. In practice, this means data are collected on a fairly evenly distributed set of lines throughout the object. The concept of complete data can be made precise using sampling theory as in [**52, 53**] and Faridani's article in these proceedings [**12**]. In this case, the commonly used reconstruction algorithm is filtered backprojection (Theorem 2.5).

Limited data tomography is tomography when the data set does not include all lines. For example, data for *region of interest tomography* (§3.2) are over lines that go through a region of interest in the object. Lines that do not meet that region are not in the data set.

2.1. General Facts about the Radon transform. In general, we will follow the notation in [**52**]. We will need to give coordinates on the unit sphere, S^1 so to each angle $\varphi \in [0, 2\pi]$, we denote the unit vector in direction φ as θ and the unit vector $\pi/2$ units counterclockwise from θ as $\theta^\perp$:

$$\theta = \theta(\varphi) = (\cos\varphi, \sin\varphi) \qquad \theta^\perp = \theta^\perp(\varphi) = (-\sin\varphi, \cos\varphi)\,. \tag{2.2}$$

We identify 0 and 2π as angles, and this allows us to identify $[0, 2\pi]$ with S^1 using the angle φ as coordinate.

We define

$$L(\varphi, s) = \{x \in \mathbb{R}^2 \,\big|\, x \cdot \theta(\varphi) = s\}$$

to be the line perpendicular to $\theta = \theta(\varphi)$ and s directed units from the origin. The line $L(\varphi, s)$ represents a line along which X-rays travel.

The Radon transform (2.3) of a function $f \in L^1(\mathbb{R}^2)$ can be naturally interpreted as a function of (φ, s):

$$Rf(\varphi, s) = \int_{x \in L(\varphi,s)} f(x)\, dx_L = \int_{t=-\infty}^{\infty} f(s\theta + t\theta^\perp)\, dt\,, \tag{2.3}$$

and in fact, R is continuous.

THEOREM 2.1. *The Radon transform is a continuous map from $L^1(\mathbb{R}^2)$ to $L^1([0, 2\pi] \times \mathbb{R})$, and for $f \in L^1(\mathbb{R}^2)$, $\|Rf\|_{L^1([0,2\pi]\times\mathbb{R})} \le 2\pi \|f\|_{L^1(\mathbb{R}^2)}$.*

The proof will be given along with the proof of Theorem 2.2.

Note that R satisfies the following evenness condition

$$Rf(\varphi, s) = Rf(\varphi + \pi, -s) \tag{2.4}$$

since $L(\varphi, s) = L(\varphi + \pi, -s)$ and dx_L is the arc-length measure. We define the backprojection operator, the dual Radon transform of $g \in L^1([0, 2\pi] \times \mathbb{R})$, as

$$R^* g(x) = \int_{\varphi=0}^{2\pi} g(\varphi, x \cdot \theta(\varphi))\, d\varphi. \tag{2.5}$$

This is the integral of g over all lines through x, since $L(\varphi, x \cdot \theta)$ is the line through x and perpendicular to θ. Let g be a smooth function of compact support, $g \in$

$C_c([0,2\pi]\times\mathbb{R})$, then the partial Fourier transform of g in the s variable is:

$$\begin{aligned}\mathcal{F}_s g(\varphi,\sigma) &= \frac{1}{\sqrt{2\pi}}\int_{s=-\infty}^{\infty} e^{-is\sigma} g(\varphi,s)\,ds,\\ \mathcal{F}_s^{-1} g(\varphi,s) &= \frac{1}{\sqrt{2\pi}}\int_{\sigma=-\infty}^{\infty} e^{is\sigma} g(\varphi,\sigma)\,d\sigma\end{aligned} \tag{2.6}$$

For $f\in C_c(\mathbb{R}^n)$ we define the n-dimensional Fourier transform and its inverse by

$$\begin{aligned}\widehat{f}(\xi) = \mathcal{F}f(\xi) &= \frac{1}{(2\pi)^{n/2}}\int_{x\in\mathbb{R}^n} e^{-ix\cdot\xi} f(x)\,dx\\ \mathcal{F}^{-1}f(x) &= \frac{1}{(2\pi)^{n/2}}\int_{\xi\in\mathbb{R}^n} e^{ix\cdot\xi} f(\xi)\,d\xi\,.\end{aligned} \tag{2.7}$$

We can now define the Riesz potential, I_s^{-1}, for $g\in C_c^\infty([0,2\pi]\times\mathbb{R})$ as the operator with Fourier multiplier $|\sigma|$:

$$I_s^{-1} g = I^{-1} g = \mathcal{F}_s^{-1}(|\sigma|\mathcal{F}_s g)\,. \tag{2.8}$$

Before we can prove the inversion formula, we need to know the fundamental relationship between the Radon and Fourier transforms.

THEOREM 2.2 (General Projection Slice Theorem, e.g., [**52, 53**]). *Let $f\in L^1(\mathbb{R}^2)$ and let $\varphi\in[0,2\pi]$. Let $h\in L^\infty(\mathbb{R})$. Then*

$$\int_{s=-\infty}^{\infty} Rf(\varphi,s)h(s)\,ds = \int_{x\in\mathbb{R}^2} f(x)h(\theta\cdot x)\,dx\,. \tag{2.9}$$

That is, integrating $Rf(\varphi,\cdot)$ with respect to $h(s)$ is the same as integrating f with respect to the plane wave in direction θ, $h(\theta\cdot x)$.

A special case of the projection-slice theorem with $\sigma\in\mathbb{R}$ and $h(s)=e^{-is\sigma}/(2\pi)$ is especially useful.

COROLLARY 2.3 (Fourier Slice Theorem). *Let $f\in L^1(\mathbb{R}^2)$. Then,*

$$\tfrac{1}{\sqrt{2\pi}}\mathcal{F}_s Rf(\varphi,\sigma) = \widehat{f}(\sigma\theta)\,. \tag{2.10}$$

This corollary shows why R is injective on domain $L^1(\mathbb{R}^2)$: if $Rf\equiv 0$, then $\widehat{f}\equiv 0$ which shows that f is zero by injectivity of the Fourier transform.

PROOFS OF THEOREMS 2.1 AND 2.2. First, we establish that R is defined and continuous from $L^1(\mathbb{R}^2)$ to $L^1([0,2\pi]\times\mathbb{R})$ using Fubini's theorem, and the General Projection Slice Theorem will follow.

Let $f\in L^1(\mathbb{R}^2)$ and let $H:[0,2\pi]\times\mathbb{R}\times\mathbb{R}\to\mathbb{R}^2$ be defined by $H(\varphi,s,t) = (s\theta(\varphi)+t\theta^\perp(\varphi))$. Then $f\circ H$ is a Lebesgue measurable function since f is measurable and H is continuous. Furthermore, for $\varphi\in[0,2\pi]$ fixed, $(s,t)\mapsto H(\varphi,s,t)$ is a rotation of $\mathbb{R}^2$, so it preserves measure. Therefore, $(s,t)\mapsto f\big(H(\varphi,s,t)\big)$ is in $L^1(\mathbb{R}^2)$ and

$$\int_{x\in\mathbb{R}^2} f(x)\,dx = \int_{s=-\infty}^{\infty}\int_{t=-\infty}^{\infty} f\big(H(\varphi,s,t)\big)\,dt\,ds \tag{2.11}$$

$$= \int_{s=-\infty}^{\infty}\int_{t=-\infty}^{\infty} f(s\theta+t\theta^\perp)\,dt\,ds \tag{2.12}$$

$$= \int_{s=-\infty}^{\infty} Rf(\varphi,s)\,ds\,. \tag{2.13}$$

The right-hand side of (2.12) consists of an inner integral in the θ direction and an integral over the set of lines perpendicular θ, and this is exactly (2.13). Note that (2.13) follows from (2.12) by the definition of R, (2.3).

Equation (2.11) implies that $f \circ H \in L^1([0,2\pi] \times \mathbb{R}^2)$ as follows.

$$\begin{aligned} \|f \circ H\|_{L^1([0,2\pi]\times\mathbb{R}^2)} &= \int_{\varphi=0}^{2\pi} \left(\int_{s=-\infty}^{\infty} \int_{t=-\infty}^{\infty} \left| f\big(H(\varphi,s,t)\big) \right| ds\, dt \right) d\varphi \\ &= \int_{\varphi=0}^{2\pi} \|f\|_{L^1(\mathbb{R}^2)}\, d\varphi \qquad (2.14) \\ &= 2\pi \|f\|_{L^1(\mathbb{R}^2)}\,. \end{aligned}$$

Now that we know $f \circ H$ is in L^1, we can use Fubini's Theorem on domain $[0,2\pi] \times \mathbb{R}^2$. Using (2.3):

$$\begin{aligned} \|Rf\|_{L^1([0,2\pi]\times\mathbb{R})} &= \int_{\varphi=0}^{2\pi} \int_{s=-\infty}^{\infty} |Rf(\varphi,s)|\, ds\, d\varphi \\ &= \int_{\varphi=0}^{2\pi} \int_{s=-\infty}^{\infty} \left| \int_{t=-\infty}^{\infty} f(s\theta(\varphi) + t\theta^{\perp}(\varphi))\, dt \right| ds\, d\varphi \\ &\le \int_{\varphi=0}^{2\pi} \int_{s=-\infty}^{\infty} \int_{t=-\infty}^{\infty} \left| f(H(\varphi,s,t)) \right| dt\, ds\, d\varphi \qquad (2.15) \\ &= 2\pi \|f\|_{L^1(\mathbb{R}^2)} \end{aligned}$$

by (2.14). This shows R is continuous in L^1.

The projection slice theorem follows from (2.11)-(2.13) and is an exercise for the reader. First, let $F(x) = f(x)h(x \cdot \theta)$, then F is in $L^1(\mathbb{R}^2)$. Now, plug F into (2.11). □

This theorem allows us to prove the easy part of the fundamental range theorem for the Radon transform. A function f is said to be in the Schwartz space $\mathcal{S}(\mathbb{R}^2)$ if and only if f is C^∞ and f and all its derivatives decrease faster than any power of $1/|x|$ at ∞. A function $g(\varphi, s)$ is said to be in the Schwartz space $\mathcal{S}([0,2\pi] \times \mathbb{R})$ if $g(\varphi, s)$ can be extended to be smooth and $2\pi-$periodic in φ, and g decreases (along with all derivatives in s) faster than any power of $1/|s|$ uniformly in φ.

THEOREM 2.4 (Range Theorem). *Let $g(\varphi, s) \in \mathcal{S}([0,2\pi] \times \mathbb{R})$ be even ($g(\varphi, s) = g(\varphi + \pi, -s)$) (see (2.4)). Then, g is in the range of the Radon transform, $g = Rf$ for some $f \in \mathcal{S}(\mathbb{R}^2)$, if and only if all of the following moment conditions hold.*

$$(2.16)\quad \forall k = 0, 1, 2, \ldots, \quad \int_{s=-\infty}^{\infty} g(\varphi, s) s^k\, ds \quad \textit{is a homogeneous polynomial of degree } k \textit{ in the coordinates of } \theta.$$

Note that the evenness condition is necessary because of (2.4). An analogous theorem is true for the Radon hyperplane transform in $\mathbb{R}^n$ [**18, 26, 27**].

PROOF SKETCH. Necessity is the easy part. We use (2.9) with $g(s) = s^k$. Then,

$$(2.17)\qquad \int_{s=-\infty}^{\infty} Rf(\varphi, s) s^k\, ds = \int_{x \in \mathbb{R}^2} f(x)(x \cdot \theta)^k\, dx$$

and expand (2.17) in the coordinates of θ. This shows (2.17) is a polynomial in θ that is homogeneous of degree k when the unit vector θ is viewed as a vector in $\mathbb{R}^2$. The difficult part of the proof is to show that if g satisfies the moment conditions, then $g = Rf$ for some f that is smooth and rapidly decreasing. One uses the Fourier Slice Theorem 2.3 to get a function f that has Radon transform g. The subtle part of the proof is to show f is smooth at the origin, and this is where the moment conditions are used. The interested reader is referred to [**18, 26, 27**] for details. □

Now we have the background to state the filtered back projection inversion formula, which will be proved at the end of the section. Recall that R^* is defined by (2.5).

THEOREM 2.5. [**70, 73, 52**] *Let $f \in C_c^\infty(\mathbb{R}^2)$. Then $f = \frac{1}{4\pi} R^*(I_s^{-1} Rf)(x)$.*

Note that this theorem is true on a larger domain than $C_c^\infty(\mathbb{R}^2)$, but even for $f \in L^1(\mathbb{R}^2)$, $I^{-1}Rf$ could be a distribution rather than a function.

The theorem is applied in practice by truncating and smoothing the multiplier $|\sigma|$ in I^{-1} and writing this truncated multiplier as a convolution operator in s [**70, 52, 53**]. The resulting approximate inversion algorithm becomes $f \approx \frac{1}{4\pi} R^*(\Phi *_s Rf)$ where Φ is the inverse Fourier transform of the truncated multiplier and $*_s$ denotes convolution in the s variable,

$$g(\varphi, \cdot) *_s h(\varphi, \cdot) = \int_{s=-\infty}^{\infty} g(\varphi, s-\tau) h(\varphi, \tau)\, d\tau\,.$$

Here is some historical background. Old X-ray CT scanners took data using this parameterization, $Rf(\varphi, s)$, so-called parallel beam data. A single X-ray emitter and detector (or parallel emitter/detector sets) were oriented perpendicular to θ and then were translated through the object (fixing φ and changing s) then rotated to a new angle and then translated. The simplest kernel Φ was given by cutting off $|\sigma|$ and taking the inverse Fourier transform of

$$\big(\mathcal{F}_s \Phi\big)(\sigma) = \begin{cases} |\sigma| & |\sigma| \le \Omega \\ 0 & |\sigma| > \Omega \end{cases}. \tag{2.18}$$

However, Φ oscillates too much (an exercise shows that $\Phi(s) = \frac{\sqrt{2}}{s^2\sqrt{\pi}}(\Omega s \sin(\Omega s) + \cos(\Omega s) - 1)$). Various approximations to (2.18) and other kernels were used. See [**73**] for a discussion of the inversion methods and kernels of that time. Data collection for these scanners was time consuming because of the translation and rotation steps, but the inversion method was a simple application of Theorem 2.5. Once $|\sigma|$ is approximated by a compactly supported function and $\Phi(s)$ is the inverse Fourier transform, then the formula can be written $f \approx \frac{1}{4\pi} R^*(\Phi *_s Rf)(x)$ and this is easy to implement since $\Phi *_s Rf$ can be done as the data are collected and the backprojection step is just averaging as θ is incremented around the circle.

Modern two-dimensional scanners take fan beam data, in which there is one point-source that emits X-rays in a fan at a bank of detectors on the other side of the body. The advantage is that the emitter/detectors need only to be rotated (not translated) to get data around the body. However, other adaptations of Theorem 2.5 are used since the data would have to be rebinned (a change of variable done) to change to the parallel beam parameterization of lines $L = L(\varphi, s)$ so the convolution

$\Phi *_s Rf(\varphi,\cdot)$ could easily be done. Modern references such as [**52, 53**] provide excellent descriptions of the new inversion methods, and a detailed description of the method is given in Alfred Louis' article in these proceedings [**44**].

PROOF OF THEOREM 2.5. The proof uses some of the key elementary formulas for the Radon transform. One writes the two-dimensional Fourier inversion formula in polar coordinates and uses Fourier Slice Theorem 2.3 to get:

$$\begin{aligned} f(x) &= \frac{1}{2(2\pi)} \int_{\varphi=0}^{2\pi} \int_{\sigma\in\mathbb{R}} e^{ix\cdot(\sigma\theta)} \widehat{f}(\sigma\theta)|\sigma|\, d\sigma\, d\varphi \\ &= \frac{1}{4\pi} \int_{\varphi=0}^{2\pi} \int_{\sigma\in\mathbb{R}} \tfrac{e^{i\sigma(\theta\cdot x)}}{\sqrt{2\pi}}|\sigma| \big(\mathcal{F}_s Rf\big)(\varphi,\sigma)\, d\sigma\, d\varphi \\ &= \frac{1}{4\pi} \int_{\varphi=0}^{2\pi} I^{-1}Rf(\varphi,\theta\cdot x)\, d\varphi = \frac{1}{4\pi} R^* I^{-1} Rf(x)\,. \end{aligned}$$

The factor of $1/2$ before the first integral occurs because the integral has $\sigma \in \mathbb{R}$ rather than $\sigma \in [0,\infty)$. □

2.2. Wavefront Sets and Singularity Detection. We will now use microlocal analysis to learn about how the Radon transform R detects singularities. To do this, we need a concept of singularity, the Sobolev wavefront set. The distribution f is in $H^\alpha(\mathbb{R}^n)$ if and only if its Fourier transform, $\widehat{f} = \mathcal{F}f$ is in $L^2(\mathbb{R}^n, (1+|\xi|^2)^\alpha)$. This relates global smoothness of f to integrability of its Fourier transform. A local version of this at a point $x_0 \in \mathbb{R}^n$ is obtained by multiplying f by a smooth cut-off function $\psi \in C_c^\infty(\mathbb{R}^n)$ (with $\psi(x_0) \neq 0$) and seeing if the Fourier transform $\widehat{(\psi f)}$ is in this weighted L^2 space. However, this localized Fourier transform $\widehat{(\psi f)}$ gives even more specific information–microlocal information–namely, the *directions* near which $\widehat{(\psi f)}$ is in $L^2(\mathbb{R}^2, (1+|\xi|^2)^\alpha)$. The precise definition is:

DEFINITION 2.6 ([**61**], p. 259). A distribution f is in *the Sobolev space* H^α *locally near* $x_0 \in \mathbb{R}^n$ if and only if there is a cut-off function $\psi \in C_c^\infty(\mathbb{R}^n)$ with $\psi(x_0) \neq 0$ such that the Fourier transform $\widehat{(\psi f)}(\xi) \in L^2(\mathbb{R}^n, (1+|\xi|^2)^\alpha)$. Let $\xi_0 \in \mathbb{R}^n \setminus 0$. The distribution f is in H^α *microlocally near* (x_0,ξ_0) if and only if there is a cut-off function $\psi \in \mathcal{D}(\mathbb{R}^n)$ with $\psi(x_0) \neq 0$ and a function $u(\xi)$ homogeneous of degree zero and smooth on $\mathbb{R}^n \setminus 0$ and with $u(\xi_0) \neq 0$ such that the product $u(\xi)\widehat{(\psi f)}(\xi) \in L^2(\mathbb{R}^n, (1+|\xi|^2)^\alpha)$. The H^α *wavefront set of* f, $\mathrm{WF}^\alpha(f)$, is the complement of the set of (x_0,ξ_0) near which f is microlocally in H^α.

Note that $\mathrm{WF}^\alpha(f)$ is conic (if $(x,\xi) \in \mathrm{WF}^\alpha(f)$ then so is $(x,a\xi)$ for any $a > 0$) and closed. Also, note that the cut-off function, ψ, makes the calculation of wavefront sets intrinsically local: one needs only values of $f(x)$ near x_0 to find the wavefront set of f above x_0.

The Sobolev wavefront set and microlocal Sobolev smoothness are usually defined on $T^*(\mathbb{R}^n)\setminus 0$, the cotangent space of $\mathbb{R}^n$ with its zero section removed, because such a definition can be extended invariantly to manifolds. To this end, let $x_0 \in \mathbb{R}^n$. If $\vec{r} = (r_1,\ldots,r_n) \in \mathbb{R}^n$, then we let $\vec{r}\mathbf{dx} = r_1\mathbf{dx}_1 + \cdots + r_n\mathbf{dx}_n$ be the cotangent vector corresponding to $\vec{r}$ in $T^*_{x_0}\mathbb{R}^n$. A basic example will give a feeling for the definition.

EXAMPLE 2.7. *Consider a function f in the plane that is smooth except for a jump singularity along a smooth curve C. Let $x \in C$ and let θ be normal to C at x. Because of this, we say that the covector $\theta\mathbf{dx}$ is conormal to C at x. Then, clearly f is not smooth at x; f is not even in H^1 locally near x. In fact, $(x, \theta\mathbf{dx}) \in \mathrm{WF}^1(f)$ and it can be shown that $\mathrm{WF}^1(f)$ is the set of all conormals to C. So, the wavefront set gives a precise concept of singularity, not only points at which f is not smooth, but also directions in which f is not smooth.*

The reader is encouraged to illustrate this principle by calculating $\mathrm{WF}^1(f)$ for the special case, $f(x,y) = \begin{cases} 0 & x < 0 \\ 1 & x \geq 0 \end{cases}$, when the curve C is the $y-$axis. This calculation is easier if one uses a cut-off function that is a product of cut-off functions in x and in y.

We will be dealing with Sobolev spaces of functions on $Y = [0, 2\pi] \times \mathbb{R}$. To do this, we extend functions $g(\varphi, s)$ on Y periodically in φ and take localizing functions ψ with support in φ less than a period so ψg can be viewed as a function on $\mathbb{R}^2$ and the two-dimensional Fourier transform can be calculated using these coordinates. We let $\mathbf{d}\varphi$ and $\mathbf{ds}$ be the standard basis of $T^*_{(\varphi,s)}([0, 2\pi] \times \mathbb{R})$, where the basis covector $\mathbf{d}\varphi$ is the dual covector to $\partial/\partial\varphi$. and $\mathbf{ds}$ is the dual covector to $\partial/\partial s$. The wavefront set is extended to distributions on $[0, 2\pi] \times \mathbb{R}$ using these local coordinates, and it is a subset of $T^*([0, 2\pi] \times \mathbb{R})$.

If the reader is not familiar with cotangent spaces, one can just envision $(x; \vec{r}\mathbf{dx})$ as the vector $(x; \vec{r})$ where x represents a point in the plane and $\vec{r}$ a tangent vector at x. In a similar way, $(\varphi, s; a\mathbf{d}\varphi + b\mathbf{ds})$ can be viewed as the vector $(\varphi, s; a, b)$.

The fundamental theorem that gives the relation between Sobolev wavefront of a function and its Radon transform is the following.

THEOREM 2.8 (Theorem 3.1 [**66**]). *Let f be a distribution of compact support, $f \in \mathcal{E}'(\mathbb{R}^2)$. Let $x_0 \in L(\varphi_0, s_0)$, $\theta_0 = \theta(\varphi_0)$, $\eta_{\mathbf{0}} = \mathbf{ds} - (x_0 \cdot \theta_0^\perp)\mathbf{d}\varphi$ and $a \neq 0$. The Sobolev wavefront correspondence is*

$$(x_0; a\theta_0\mathbf{dx}) \in \mathrm{WF}^\alpha(f) \quad \text{if and only if} \quad (\varphi_0, s_0; a\eta_{\mathbf{0}}) \in \mathrm{WF}^{\alpha+1/2}(Rf)\,. \tag{2.19}$$

Given $(\varphi_0, s_0; a\eta_{\mathbf{0}})$, $(x_0; a\theta_0\mathbf{dx})$ is uniquely determined by (2.19)*. Sobolev singularities of Rf above (φ_0, s_0) give no stable information about Sobolev singularities of f above points not on $L(\varphi_0, s_0)$ or at points on this line in directions not conormal to the line. These other singularities are smoothed by data Rf near (φ_0, s_0). Singularities above points not on the line do not affect singularities of Rf on (φ_0, s_0).*

The proof of this theorem is in the appendix along with proofs that R and R^* are elliptic Fourier integral operators and R^*R is an elliptic pseudodifferential operator.

Theorem 2.8 allows one to understand what R does to singularities in a precise and rigorous way and it provides an application of microlocal analysis to tomography. It gives an exact correspondence between singularities of f and those of Rf. Moreover, it states that the singularities of Rf that are detected from the data are of Sobolev order $1/2$ smoother than the corresponding singularities of f. A simple illustration will give an intuitive feeling for the theorem.

EXAMPLE 2.9. *Let $f : \mathbb{R}^2 \to \mathbb{R}$ be equal to one on the unit disk and zero outside. Then, $Rf(\varphi, s) = 2\sqrt{1 - s^2}$ for $|s| \leq 1$ and $Rf(\theta, s) = 0$ for $|s| > 1$. The only lines*

where Rf is not smooth are those with $|s| = 1$ and these lines are tangent to the unit circle, the curve on which f is discontinuous. Since $\mathrm{WF}^1(f)$ is the set of covectors conormal to the unit circle (see Example 2.7), singularities of Rf precisely locate the corresponding singularities of f.

REMARK 2.10. Here is how to use Theorem 2.8 to determine $\mathrm{WF}^\alpha(f)$. Let $x_0 \in \mathbb{R}^2$, and $\varphi_0 \in [0, 2\pi]$ and $a \neq 0$. To see if $(x_0, a\theta_0\mathbf{dx}) \in \mathrm{WF}^\alpha(f)$ we need to know if the covector $\big(\varphi_0, x_0\cdot\theta_0; a(\mathbf{ds} - (x_0\cdot\theta_0^\perp)\mathbf{d}\varphi)\big) \in \mathrm{WF}^{\alpha+1/2}(Rf)$. To determine this, we need only data Rf near (φ_0, s_0) where $\theta_0 = \theta(\varphi_0)$, $s_0 = x_0 \cdot \theta_0$ because the calculation of wavefront sets is local.

It follows from Theorem 2.8 that if Rf is in $H^{\alpha+1/2}$ near (φ_0, s_0), then f is H^α in directions $\pm\theta_0$ at all points on the line $L(\varphi_0, s_0)$, and if Rf is not in $H^{\alpha+1/2}$ near (φ_0, s_0), then at some point $x \in L(\varphi_0, s_0)$, (x, θ_0) or $(x, -\theta_0)$ is in $\mathrm{WF}^\alpha(f)$.

We will apply this theorem to limited data sets, that is $Rf(\varphi, s)$ for (φ, s) in an open proper subset of $\mathcal{A} \subset [0, 2\pi] \times \mathbb{R}$. With limited data in $\mathcal{A}$, the only points at which we can find wavefront sets are points $x \in L(\varphi, s)$ for $(\varphi, s) \in \mathcal{A}$, and if $x \in L(\varphi, s)$ the only wavefront directions we see at x are the directions perpendicular to the line, directions $\pm\theta$. Other wavefront directions at points on $L(\varphi, s)$ are not visible from this data, and wavefront at points off of $L(\varphi, s)$ are not visible from this data since they do not affect this data.

DEFINITION 2.11. We will say a singularity of f $(x, \pm\theta\mathbf{dx})$ is *visible* from a limited data set if the line $L(\varphi, x \cdot \theta)$ is in the data set. Other singularities will be called *invisible*.

Of course, visible singularities at a point x are ones that, according to (2.19), affect the smoothness of Rf near $(\varphi_0, x \cdot \theta_0)$. The associated singularities of Rf are 1/2 order smoother in Sobolev scales than the corresponding singularities of f, so they should be stably detectable from Radon data for lines near $L(\varphi, x \cdot \theta)$. Invisible singularities are not really invisible but are harder to reconstruct because they are smoothed to C^∞ by data near $(\varphi_0, x \cdot \theta_0)$. A similar definition was given by Palamodov [**58**] for sonar. We now illustrate the idea by an example.

EXAMPLE 2.12. *Assume we are given limited tomographic data of a function f over an open set $\mathcal{A} \subset Y$. Assume f has a jump singularity along a smooth curve C, and $x \in C$. Let θ be perpendicular to the curve C at x. Then, the line $L(\varphi, x\cdot\theta)$ is tangent to C at x and, as noted in Example 2.7, $(x, \theta\mathbf{dx}) \in \mathrm{WF}^1(f)$. If this line $L(\varphi, x\cdot\theta)$ is in the data set, i.e., $(\varphi, x\cdot\theta) \in \mathcal{A}$, then according to Theorem 2.8, this singularity at x will be stably detectable from the data, but if the line is not in the data set, then the singularity will not be stably detectable but will be smoothed by the data Rf on $\mathcal{A}$.*

In other words, if the line tangent to C at x is in the data set, then the jump singularity at x along C will be visible and if not, the singularity will be invisible.

One can use this paradigm to understand which singularities of an object will be visible from limited data, and we will illustrate this for three limited data problems in Section 3. Palamodov stated a closely related idea in [**57**]. The "tangent casting" effects of [**74**] are related to Example 2.12.

REMARK 2.13. It is important to note that this paradigm explains only part of the issue. A good algorithm should be able to reconstruct singularities more clearly

if they are visible from the data set. But other issues, such as noisy data or a bad algorithm, could have a larger effect on the reconstruction than the paradigm. In any case, the paradigm does not predict how an algorithm will reconstruct invisible singularities. Some algorithms, like my ERA [**67**] (see Figure 1) smear these singularities and others, like limited data Lambda CT can just make them disappear (e.g., [**37**]). Finally, other issues such as data sampling can have a dramatic effect on reconstruction as will be discussed in Faridani's article [**12**] in this collection.

Now, we will give some history of the microlocal perspective on Radon transforms. Guillemin first developed the microlocal analysis of the Radon transform. In broad generality, he proved that R is an elliptic Fourier integral operator, and he proved that R^*R is an elliptic pseudodifferential operator under a specific assumption, the Bolker Assumption (see Remark A.3) [**22**]. Because Guillemin showed R is a Fourier integral operator associated to a specific canonical relation (A.6) [**22, 24**], (2.19) follows. Sobolev continuity is a basic property for Fourier integral operators; any FIO, such as R, of order $-1/2$ will map functions in H^α of fixed compact support continuously to functions in $H^{\alpha+1/2}_{\text{loc}}$. If the operator is elliptic, then the original function must be $1/2$ order less smooth than its image. Theorem 2.8 is a refinement of this observation. Not only does R smooth of order $1/2$ but it maps functions that are in H^α microlocally near a given covector to functions that are in $H^{\alpha+1/2}$ near the covector given by the correspondence (2.19).

The author [**62**] described the symbol of R^*R for all generalized Radon transforms satisfying the Bolker Assumption (see Remark A.3) in terms of the measures involved into the transform. He also proved more concrete results for the hyperplane transform. Beylkin [**3**] proved related results for Radon transforms satisfying the Bolker Assumption integrating over surfaces in $\mathbb{R}^n$. One type of generalized Radon transform will be discussed in Peter Kuchment's article in these proceedings [**36**].

The author's article [**66**] that included Theorem 2.8 was written to show the connection between microlocal analysis and singularity detection in tomography. The microlocal analysis was known to Fourier analysts, and tomographers understood the heuristic ideas about singularity detection, but the explicit and precise connection in (2.19) was not generally known in tomography. Subsequent many authors have used microlocal analysis to understand problems in tomography including radar [**54, 55**], and X-ray tomography (e.g., [**37, 33**]).

3. Limited Data Tomography

Limited tomographic data are tomographic data given on some proper open subset $\mathcal{A} \subset [0, 2\pi] \times \mathbb{R}$. Theorem 2.8 and Remark 2.10 provide a paradigm to decide which singularities of f are stably visible from limited tomographic data, and we will examine what this predicts for three common types of limited data: exterior CT, (§3.1), the interior problem or region of interest CT (§3.2), and limited angle region of interest CT (§3.3).

Density functions f in tomography can often be modelled by piecewise continuous functions that are continuous on open sets with well-behaved boundaries. So, singularities of f occur at the boundaries, and the singularities are in $H^{1/2-\epsilon}$ for $\epsilon > 0$. By Theorem 2.8, the corresponding singularities of the Radon data Rf will be in $H^{1-\epsilon}$. A limitation of this analysis is that any discrete data Rf can

be considered an approximation of a smooth function. However, singularities of Rf should have large norm in H^1 when given by discrete data and so should be visible. Moreover, the paradigm of the preceding section is observed in all typical CT reconstructions from limited data including those in Figures 1, 2, and 3 below.

We now give a little historical perspective. Ramm and Zaslavsky [**71**] have analyzed how the Radon transform itself behaves on functions that are smooth except at smooth boundary surfaces. They give precise asymptotics of Rf at lines tangent to boundaries depending on the curvature of the boundaries, and they have proposed a singularity detection method using this information on the raw data [**71**]. This method has been tested on simulated data [**34**]. A more general method using wavefront sets has been proposed [**66**] based on correspondence (2.19) and Theorem 2.8. Candès and Donoho, have developed ridgelets [**5**], an exciting way to make this correspondence and wavefront sets in general numerically tractable [**6**].

It should be pointed out that one can also understand stability of limited data tomography using singular value decompositions [**9, 49, 43, 46, 47, 48**], and they reflect the principle predicted by the microlocal analysis: singular functions associated with large singular values (which are easy to reconstruct) oscillate in directions in which wavefront is easily detectable, and vice versa. This is discussed more completely in [**68**] and examples are given there.

3.1. The Exterior Problem. Let $M > 1$ and assume $\operatorname{supp} f \subset \{x \in \mathbb{R}^2 \big| |x| \leq M\}$. In the exterior problem, one has data $Rf(\varphi, s)$ for all $\varphi \in [0, 2\pi]$ but only for $|s| > 1$. By the support theorem for the Radon transform [**18, 26**], one can reconstruct $f(x)$ for $|x| > 1$. This problem comes up in studies of the solar corona [**1**] in which data are total intensities of the corona of the sun along lines exterior to the core of the sun that go from the solar corona to the observer on earth. Exterior data also occur in industrial tomography of very large objects such as rocket shells, for which X-ray data through their centers is too highly attenuated to be usable [**67**].

Here is some history. An example of Finch's can be adapted to show inversion of the exterior transform is discontinuous in any range of Sobolev norms. This is reflected in the fact that some singularities are invisible; exterior data smooths them. Lissianoi [**40**] has extended Finch's Sobolev discontinuity result to show that in the exterior problem even recovery of the function in a smaller ring than where the data are given and does not improve stability. However, logarithmic stability has been proved by Isakov and Sun [**31**].

Lewitt and Bates [**2**], Louis, and Natterer [**51**] have developed good reconstruction algorithms that use exterior data. Lewitt and Bates' algorithm completes the exterior data by projecting it on the range of the complete Radon transform as Louis did for limited angle data [**42**]. The projection step is unstable because the singular functions are not orthogonal on the annulus but on a disk. Natterer's algorithm is an effective regularization method.

The author has developed an exterior reconstruction algorithm which employs a singular value decomposition [**60**] for the Radon transform on domain $L^2(\{x \in \mathbb{R}^2 \big| |x| \geq 1\})$ and *a priori* information about the shape of the object to be reconstructed. Reconstructions for 'medical' phantoms are given in Figure 1 [**63**], and reconstructions from industrial phantoms are in [**65, 64**] and real industrial data in [**67**]. Industrial reconstruction from the author's limited angle exterior

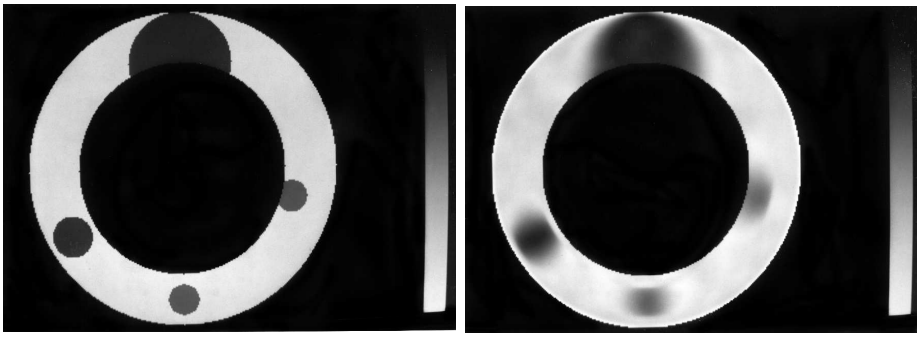

Figure 1. Phantom (left) and reconstruction (right) from simulated data [**63**] using the author's exterior reconstruction algorithm. Note how the boundaries tangent to lines in the data set (lines not intersecting the inner disk) are sharper than boundaries tangent to lines not in the data set.

Lambda tomography algorithm [**68**] are given in Figure 2. The article [**37**] has Lambda reconstructions of simulated exterior data.

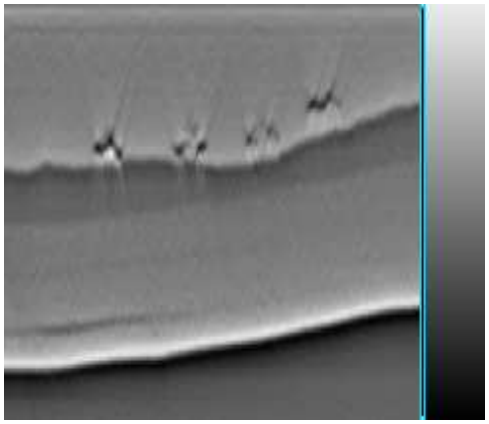

Figure 2. Polar coordinate display of the author's limited angle exterior Lambda reconstruction from a $3\pi/4$ angular range limited angle exterior data set of a Perceptics rocket motor mockup [**68**]. The horizontal axis corresponds to $\varphi \in [0, \pi/2]$, the vertical corresponds to $r \in [0.9453, 1.0]$ (with $r = 1$ at the bottom and magnified by a factor of 27). The bottom of the picture shows some area outside the object. The part of the reconstruction in $[\pi/2, 3\pi/4]$ is of the same quality but less interesting. Data were taken over 1350 sources in the range $[0, 3\pi/4]$ and 280 detectors.

The reconstructions in Figures 1 and 2 illustrate the paradigm in Remark 2.10 perfectly. The lines in the data set are those that do not meet the center disk, and the boundaries tangent to those lines (with wavefront perpendicular to those lines) are better defined than other parts of the boundaries. For example, in Figure 1, for each little circle, the inside and outside boundaries are better defined than the sides. The reconstruction in Figure 2 is displayed in polar coordinates, and if it is mapped into rectangular coordinates, almost all of the singularity curves are tangent to lines in the data set since the vertical axis is the radial direction so these curves map to curves of approximately constant radius.

3.2. Region of Interest Tomography. Let $M > 1$ and assume $\operatorname{supp} f \subset \{x \in \mathbb{R}^2 \big| |x| \leq M\}$. *Region of interest data* (or *interior tomographic data*) are data $Rf(\varphi, s)$ for all φ but only for $|s| < 1$. Data are missing over lines outside the unit disk, even though $\operatorname{supp} f$ can meet the annulus $\{x \in \mathbb{R}^2 \big| 1 \leq |x| \leq M\}$. This is the opposite of exterior data, in which data are given *outside* the unit disk.

The goal of region of interest CT is to reconstruct information about $f(x)$ in the region of interest, the unit disk. This problem comes up whenever scientists want information only about some region of interest in an object, not the whole object, or in problems, such as high-resolution tomography of very small parts of objects, for which it is difficult or impossible to get complete high-resolution CT data [**14**].

Simple examples (derived using Range Theorem 2.4) show the interior transform, the Radon transform with this limited data, is not injective.

However, according to Theorem 2.8, all singularities of f in $|x| < 1$ are visible. To see this, choose a point x inside the unit disk and choose an angle $\varphi \in [0, 2\pi]$. Then the line through x and normal to $\theta = \theta(\varphi)$ is in the data set for interior tomography. Therefore, by Theorem 2.8, any singularity of f at $(x; \theta \mathbf{dx})$ is stably detected by interior data. This explains why singularity detection methods work so well for interior data.

Lambda tomography [**73, 15, 13, 78**] is a well developed singularity detection algorithm that uses interior data. The key is that by (2.8), $I^{-2} = I^{-1} \circ I^{-1} = -\frac{d^2}{ds^2}$ which is a local operator. In Lambda tomography, one replaces I^{-1} in the filtered backprojection inversion formula, $f = \frac{1}{4\pi} R^* I^{-1} Rf$ by I^{-2} to get

$$\sqrt{-\Delta} f = \frac{1}{4\pi} R^* I^{-2} Rf = \frac{-1}{4\pi} R^* (\tfrac{d^2}{ds^2} Rf)\,. \tag{3.1}$$

One shows the first equality in (3.1) using arguments similar to those in the proof of Theorem 2.5. Equation (3.1) is a local reconstruction formula because one needs only data Rf near $(\varphi, x \cdot \theta)$ to calculate $\frac{d^2}{ds^2} Rf(\varphi, x \cdot \theta)$ and then to calculate $\frac{-1}{4\pi} R^* \big(\frac{d^2}{ds^2} Rf(x)\big)$. Moreover, $\sqrt{-\Delta}$ is an elliptic pseudodifferential operator of order 1 and so $\mathrm{WF}^{\alpha}(f) = \mathrm{WF}^{\alpha-1}(\sqrt{-\Delta} f)$. This reconstruction formula takes singularities of f and makes them more pronounced; any WF^{α} singularity of f becomes a more pronounced singularity, in $\mathrm{WF}^{\alpha-1}$, because Λ is an elliptic pseudodifferential operator of order 1. At the same time, there is a cupping effect at the boundaries [**15**]. Because of this, the developers of Lambda CT chose to add a multiple of $R^* Rf = f * (2/|x|)$ (see the proof of Theorem A.1) to the reconstruction. The effect is to provide a smoothed version of the density f; moreover, with a good multiple, the cupping effects are decreased [**15, 13**].

Here is some background and perspective. The authors of [**2**] have developed a reconstruction method that projects the interior data onto the range of the Radon transform with complete data and then inverts this completed data. Because of the non-uniqueness of the problem, this projection step is not unique. Maaß has developed a singular value decomposition for this problem, and he showed that singular functions associated to small singular values are fairly constant inside the region of interest, the unit ball [**48**]. These singular functions corresponding to small singular values are difficult to reconstruct, but they do not add much detail inside the region since they are relatively constant there. See also [**46**]. This

reflects the fact that all Sobolev singularities inside the region of interest are stably reconstructed.

Limited angle and exterior versions of Lambda CT have been developed, and they are promising on simulations [**37**] and tests on industrial and electron microscope data (see [**68**] and Section 3.3).

Other algorithms for region of interest CT have been developed. Ramm and Katsevich developed pseudolocal tomography [**35**]. In industrial collaboration, Louis has used wavelets to help detect boundaries of bone and metal in X-ray CT. Madych [**50**] used wavelet analysis to show the strong relationship between Lambda CT, pseudolocal CT, and regular filtered backprojection. Authors of the papers [**10, 72**] have also used wavelet techniques for local tomography. They use Radon data to calculate wavelet coefficients of the density to be reconstructed. Although they need some data slightly outside the region of interest, their methods are fairly local.

Candès and Donoho [**5**] have recently defined ridgelets, wavelets that are not radially symmetric and are more sensitive to singularities in specified directions. They have developed a local tomographic reconstruction algorithm using ridgelets that provides high-quality reconstructions in practice. Their ideas reflect the singularity detection predictions of Theorem 2.8. In an exciting development, they have also used wavelets to detect wavefront sets of functions and develop a ridgelet theory of Fourier integral operators [**6**].

For the X-ray transform over a curve in $\mathbb{R}^3$, Louis and Maaß [**45**] have developed a very promising generalization of Lambda CT (see [**33**] for related ideas). Greenleaf and Uhlmann [**20, 21**] completely analyzed the microlocal properties of R^*R for admissible transforms on geodesics, including this case. The microlocal analysis of this three-dimensional X-ray transform has been investigated by Finch, Lan, and Uhlmann [**16, 39**], and Katsevich [**33**]. The operator $R^*I^{-2}R$ adds singularities to f because R is not well enough behaved; for the classical line transform in the plane, $R^*I^{-2}R$ is an elliptic pseudodifferential operator and therefore preserves singularities. The theorem corresponding to Theorem 2.8 for the X-ray transform on lines through a curve is given in [**66**], and it explains which singularities are stably reconstructed by this transform. The prediction is observed in the reconstructions in [**45**]. The general analysis in [**23**] provides the basic microlocal results needed to prove this theorem, and the specific microlocal properties of this operator on manifolds is given [**20**]. The microlocal properties of this line transform were also developed in [**4**] as a way to prove support and uniqueness theorems for the X-ray transform.

3.3. Limited angle region of interest tomography and electron microscopy. Disregarding scatter and assuming an ideal detector, one can interpret electron microscope data as the X-ray transform of the three-dimensional structure of the object being scanned [**17, 28, 53**]. In collaboration with Ulf Skoglund at the Karolinska Institute and Ozan Öktem at Sidec Technologies, the author is developing a limited data singularity detection algorithm [**68**] for electron microscopy data. The starting point is the author's adaptation of Lambda tomography to limited data (see [**68**] for exterior and limited angle exterior data and see [**37**] for a related algorithm for general measures).

Here is some background on other tomographic methods in electron microscopy. It should be pointed out that there is a rich theory that considers electron microscopy as a discrete problem. In one model, the goal is to find the location of atoms and the model is a pixel function that is either one or zero. Authors such as Lohmann (Ph.D. Thesis, Uni. Münster), Shepp and others have developed good methods to detect such objects using data from a few angles. In another type of experiment, so called single-view microscopy, the object consists of multiple copies of the same rigid (typically crystalline) molecule, and the goal is to reconstruct the shape of the molecule from one view of the sample. In this case, the data are images of the same molecule in different *but unknown* directions. Researchers (e.g., [**19**]) have developed methods to reconstruct structures from projections in random directions.

However, our model is more intrinsically integral geometric. The Karolinska Institute has an electron microscope which images the specimen in a stack of two-dimensional slices. One can rotate the object in a limited angular range in the microscope, typically 120°, so these data are so called *limited angle tomographic data*. This method takes tomographic data of individual molecules from different, known angles, and the result is a reconstruction of the specific molecules. As opposed to the "discrete" methods above, this method can image individual molecules among many, varied objects and find how each is shaped.

Furthermore, the sample is so long relative to the thin focused electron beam that only a small region of interest is being imaged. Therefore the data are limited angle region of interest data

Ulf Skoglund and coresearchers at Karolinska Institute have developed a constrained minimum relative entropy method of reconstruction [**56**]. This method works by starting with a prior, which is a guess for the object to be reconstructed, and my algorithm could be used as such a prior, or as an independent reconstruction method.

Let V be the region of interest, a small open set in a cross-section of the slide, and let U be the set of perpendicular directions the microscope is rotated in angles. So, the data set consists of lines for $\{(\varphi, x\cdot\theta) \,\big|\, \varphi \in U, x \in V\}$. If we apply Theorem 2.8 and Remark 2.10, the only wave front directions of f at points $x_0 \in V$ we will be able to see are those with directions $\varphi \in U$.

The visible singularities (those tangent to lines in the data set [**66**], Remark 2.10 and Example 2.12) should be precisely reconstructed by the algorithm. Two of my reconstructions are given in Figure 3. The left picture is a reconstruction of a virus from relatively clean data, and the right one uses very noisy simulated data of the cross-section of a spherical shell. The left reconstruction used higher electron flux than is typical (making for less noise and easier reconstruction), and the mottling in the right reconstruction is typical of reconstructions of real data with lower electron flux. Both reconstructions illustrate the principle that object boundaries tangent to lines in the data set (lines with perpendicular angle between 30° and 150°) are well imaged, and others are not.

Appendix A. The microlocal properties of R and R^*R

In this section, we will show that R^*R is an elliptic pseudodifferential operator and then that R and R^* are elliptic Fourier integral operators. In the process, we

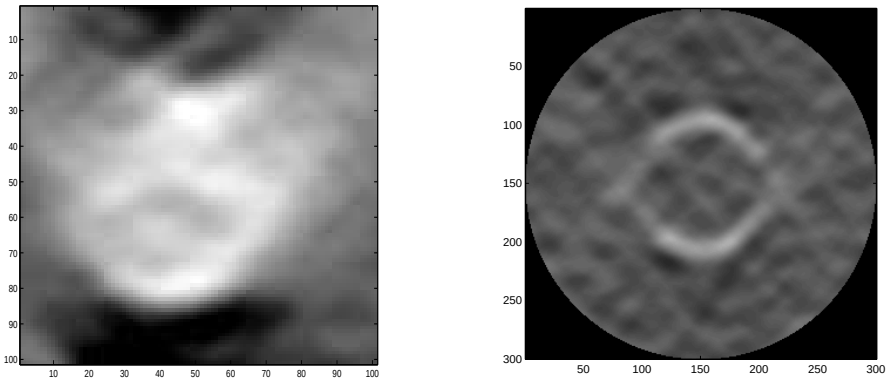

Figure 3. Left: reconstruction from my local tomography algorithm of virus from clean data. Right: reconstruction using the same algorithm of a cross-section of a sphere from very noisy simulated data, both from the Karolinska Institute and Sidec. In both pictures the visible singularities (those with normal angles between 30° and 120°) are better reconstructed.

will calculate their canonical relations. Finally, we will use these results to prove Theorem 2.8.

THEOREM A.1. *R^*R is an elliptic pseudodifferential operator of order -1 and*

$$R^*Rf(x) = \int_{\xi\in\mathbb{R}^2} e^{ix\cdot\xi}\frac{2}{|\xi|}\widehat{f}(\xi)\,d\xi\,. \tag{A.1}$$

PROOF. Here is a fun exercise for the reader. Show

$$R^*Rf(x) = \Big(\frac{2}{|x|}\Big) * f\,. \tag{A.2}$$

One can begin the proof with the fact $Rf(\varphi, x_0\cdot\theta) = \int_{t=-\infty}^{\infty} f(x_0 + t\theta^\perp)\,dt$ and then use polar coordinates.

Next, we use the fact that the Fourier transform of $1/|x|$ is $1/|\xi|$ [**27**, (42) p. 161]. Now, we take the Fourier transform and then inverse Fourier transform of (A.2) to get

$$R^*Rf(x) = 2\pi\mathcal{F}^{-1}\Big(\frac{2}{|\xi|}\widehat{f}\Big) = \int_{\xi\in\mathbb{R}^2} e^{ix\cdot\xi}\frac{2}{|\xi|}\widehat{f}(\xi)\,d\xi \tag{A.3}$$

which proves (A.1). The factor of 2π in front of the middle term in (A.3) comes about because, with our normalizations, $\mathcal{F}(f*g) = 2\pi(\mathcal{F}f)(\mathcal{F}g)$. Note that the integral is in L^1 for $f\in C_c^\infty(\mathbb{R}^2)$ and it can be defined more generally, as with pseudodifferential operators, using integration by parts [**61**]. Because the symbol of R^*R, $\frac{2}{|\xi|}$, is homogeneous and nowhere zero, R^*R is a classical elliptic pseudodifferential operator [**61**]. Because the symbol is homogeneous of degree -1, R^*R is a pseudodifferential operator of order -1. □

Our theorems about the Radon transform itself will be easier to describe if we recall our identification on $[0,2\pi]$. We have identified 0 and 2π so $\varphi\in[0,2\pi]$ becomes a smooth coordinate on S^1, and we let

$$y = (\varphi, s)\in Y := [0,2\pi]\times\mathbb{R}\,. \tag{A.4}$$

We denote the dual covector to $\partial/\partial\varphi$ by $\mathbf{d}\varphi$, and we denote covectors in $T^*\mathbb{R}^2$ by $(r_1, r_2)\mathbf{dx} = r_1\mathbf{dx}_1 + r_2\mathbf{dx}_2$. Rf is a function of $y = (\varphi, s) \in Y$, $Rf(y) = Rf(\varphi, s)$.

We need some notation about subsets of vector bundles. Let X and Y be manifolds and let $A \subset T^*X \times T^*Y$, then we define

$$\begin{aligned} A' &= \{(x, y; \xi, -\eta) \,\big|\, (x, y; \xi, \eta) \in A\}, \\ A^t &= \{(y, x; \eta, \xi) \,\big|\, (x, y; \xi, \eta) \in A\}. \end{aligned}$$

If, in addition, $B \subset T^*Y$ then

$$A \circ B = \{(x, \xi) \in T^*X \,\big|\, \exists (y, \eta) \in B \text{ such that } (x, y; \xi, \eta) \in A\} \tag{A.5}$$

THEOREM A.2. *R is an elliptic Fourier integral operator (FIO) of order $-1/2$ and with canonical relation*

$$C = \{(x, \varphi, s; a(\theta\mathbf{dx} + \mathbf{ds} - (x \cdot \theta^\perp)\mathbf{d}\varphi) \,\big|\, a \neq 0,\ x \cdot \theta = s\}\,. \tag{A.6}$$

The projection $p_Y : C \to T^*Y$ is an injective immersion. Therefore, C is a local canonical graph [**77**, Chapter VIII, §6].

R^* is an elliptic Fourier integral operator of order $-1/2$ and with local canonical graph C^t.

The canonical relation of a FIO is used to tell the microlocal properties of a FIO including what it does to singularities, and we will use it in our calculation in our proof of Theorem 2.8 at the end of the appendix.

PROOF. First, we will use the Fourier-Slice Theorem 2.3 to show R is an elliptic FIO. Define the "polar projection" $J : C^\infty(\mathbb{R}^2) \to C^\infty([0, 2\pi] \times \mathbb{R})$ by $Jf(\varphi, s) = f(s\theta)$. We take the one-dimensional inverse Fourier transform in (2.10):

$$\begin{aligned} Rf(\varphi, s) &= \mathcal{F}_s^{-1}\mathcal{F}_s Rf(\varphi, s) \\ &= \sqrt{2\pi}(\mathcal{F}_s^{-1} \circ (J \circ \mathcal{F}_{x\to\xi}))(f)(\varphi, s) \\ &= \frac{1}{2\pi}\int_{\sigma=-\infty}^{\infty}\int_{x\in\mathbb{R}^2} e^{i(s-\theta\cdot x)\sigma} f(x)\, dx\, d\sigma\,. \end{aligned} \tag{A.7}$$

Of course, this integral does not converge absolutely, although the operation $\mathcal{F}^{-1}_{\sigma\to p} \circ J \circ \mathcal{F}_{x\to\xi}$ is defined for $f \in C_c^\infty(\mathbb{R}^2)$. To make the integrals converge, one does integrations by parts as with Fourier integral operators in general to show (A.7) can be defined on distributions [**30, 76**]. Equation (A.7) shows that R is an elliptic Fourier integral operator with phase function $\phi(x, \varphi, s, \sigma) = (s - \theta\cdot x)\sigma$ and amplitude $1/2\pi$.

To calculate the canonical relation for R, we follow the general methods in [**30**, p. 165] or [**77**, (6.1) p. 462]. We first calculate the differentials of ϕ,

$$d_x\phi = -\sigma\theta\mathbf{dx}, \qquad d_y\phi = \sigma(\mathbf{ds} - x \cdot \theta^\perp\mathbf{d}\varphi) \qquad d_\sigma\phi = (s - x \cdot \theta)\mathbf{d}\sigma\,. \tag{A.8}$$

Next we define an auxiliary manifold Σ_ϕ, the set of points at which $d_\sigma\phi = 0$:

$$\Sigma_\phi = \{(x, \varphi, s, \sigma) \in \mathbb{R}^2 \times Y \times (\mathbb{R} \setminus \{0\}) \,\big|\, s - x \cdot \theta = 0\}\,. \tag{A.9}$$

The set

$$Z = \{(x, \varphi, s) \in \mathbb{R}^2 \times Y \,\big|\, s - x \cdot \theta = 0\} \tag{A.10}$$

is called the *incidence relation of R* because it is the set of all (x, φ, s) with $x \in L(\varphi, s)$, and it is the projection of Σ_ϕ on the first coordinates.

Note that the conditions for ϕ to be a nondegenerate phase function [**77**, (2.2)-(2.4), p. 315] hold because $d_x\phi$ and $d_y\phi$ are not zero for $\sigma \neq 0$. Therefore R is a

Fourier integral operator. R has order $-1/2$ because its symbol $1/2\pi$ is homogeneous of degree zero, $2 = \dim \mathbb{R}^2 = \dim Y$, and σ is one dimensional (see [**77**, p. 462 under (6.3)]). Since the symbol, $1/2\pi$, is homogeneous and nowhere zero, R is elliptic.

The canonical relation, C associated to R is defined by the map

$$\Sigma_\phi \ni (x, \varphi, s, \sigma) \mapsto (x, \varphi, s; d_x\phi, -d_y\phi) \in C\,.$$

Therefore,

$$C = \{(x, \varphi, s; -\sigma(\theta \mathbf{dx} + \mathbf{ds} - (x \cdot \theta^\perp)\mathbf{d}\varphi) \,\big|\, s - x \cdot \theta = 0, \sigma \neq 0\}\,. \tag{A.11}$$

The equation (A.6) is gotten from (A.11) by letting $a = -\sigma$.

To show the projection $p_Y : C \to T^*Y$ is an injective immersion, we need only observe that the second coordinates in (A.6), $(\varphi, s, a(\mathbf{ds} - x \cdot \theta^\perp \mathbf{d}\varphi))$, determine the factor a (from the **ds** coordinate) and since $a \neq 0$, these coordinates smoothly determine x by $x = (x \cdot \theta^\perp)\theta^\perp + s\theta$. Since this projection is an injective immersion, the projection to $T^*\mathbb{R}^2$ is also an immersion. This can also be seen by a direct calculation showing that $p_X : C \to T^*\mathbb{R}^2$ is a two-to-one immersion (see Remark A.4). Since these projections are immersions, C is a local canonical graph and the properties of FIO associated to local canonical graphs are easier to prove (see the discussion in [**77**, Chapter VIII, §6]).

The proof for R^* is similar and will be outlined. We let $g \in C_c^\infty(Y)$ and calculate $\mathcal{F}_s^{-1}\mathcal{F}_s g$ evaluated at $(\varphi, x \cdot \theta)$ and finally integrate with respect to φ:

$$\begin{aligned} R^*g(x) &= \int_{\varphi\in[0,2\pi]} g(\varphi, x\cdot\theta)\, d\varphi \\ &= \int_{\varphi\in[0,2\pi]} \int_{\sigma=-\infty}^{\infty} \int_{s=-\infty}^{\infty} \frac{e^{i(x\cdot\theta)\sigma}}{\sqrt{2\pi}} \frac{e^{-is\sigma}}{\sqrt{2\pi}} g(\varphi, s)\, ds\, d\sigma\, d\varphi \qquad \text{(A.12)} \\ &= \int_{\varphi\in[0,2\pi]} \int_{\sigma=-\infty}^{\infty} \int_{s=-\infty}^{\infty} e^{i((x\cdot\theta)-s)\sigma} \frac{1}{2\pi} g(\varphi, s)\, ds\, d\sigma\, d\varphi\,. \end{aligned}$$

Note that the integrals can be made to converge using integration by parts arguments as with (A.7). Thus, the phase function of R^* is $\widetilde{\phi}(\varphi, s, x, \sigma) = (x \cdot \theta - s)\sigma$ and the arguments showing R is an elliptic FIO of order $-1/2$ associated to C show R^* is an elliptic FIO of order $-1/2$ associated to C^t. □

Remark A.3. It should be pointed out that since R is a FIO associated to C, it is immediate that its adjoint is a FIO associated to C^t [**30**, Theorem 4.2.1], however we gave our direct proof for R^* because it is so is elementary. Note also that the Schwartz Kernel of R (and of R^*) as a distribution on $\mathbb{R}^2 \times Y$ is the set Z in (A.10). Such distributions (including all Radon transforms [**22**]) are called conormal distributions, and their properties as Fourier integral distributions are especially simple. Note that the Lagrangian manifold of a Fourier integral operator is just the "prime," (A.5), of its canonical relation, and sometimes one associates FIO to their Lagrangian manifolds rather than their canonical relations. In fact, the Lagrangian manifold of R is $C' = N^*Z \setminus \{0\}$ (e.g., [**62**, pp. 335-337]).

We showed that the projection from C to T^*Y is an injective immersion, and this assumption is called the *Bolker Assumption* [**24**, pp. 364-365], [**62**, equation (9)]. If a generalized Radon transform satisfies this assumption, then one can compose R^* and R and show R^*R is an elliptic pseudodifferential operator. See

[**29**, Theorem 4.2.2], and discussion at the bottom of p. 180 for how to compose FIO and [**24**] [**62**] for this specific result.

PROOF OF THEOREM 2.8. The relationship (2.19) follows from the following general fact about what FIO do to wavefront sets. Let X and Y be manifolds and let S be a Fourier integral operator of order m associated to canonical relation $C \subset (T^*X \setminus \{0\}) \times (T^*Y \setminus \{0\})$. Let $f \in \mathcal{E}'(X)$, and $s \in \mathbb{R}$. Then, there is a natural relation between singularities of f and those of Sf:

$$\mathrm{WF}^{\alpha-m}(Sf) \subset (C^t) \circ \mathrm{WF}^{\alpha}(f). \tag{A.13}$$

Relation (A.13) for the C^∞ wavefront set is known (e.g., [**77**, Theorem 5.4, p. 461]). Sobolev continuity of S from $H^\alpha_c(X)$ to $H^{\alpha-m}_{\mathrm{loc}}(Y)$ is also known [**77**, Theorem 6.1, p. 466], and elementary proofs exist for global Sobolev continuity for R and R^{-1} (e.g., [**41, 25, 52**]). To prove (A.13) for Sobolev wavefront, one uses pseudodifferential operators of order zero to microlocalize near a specific cotangent direction in T^*X, L_X and in directions in T^*Y that correspond by C^t, L_Y. Then, the microlocalized operator $L_Y S L_X$ is of order m and smoothing away from these directions.

We apply this theorem to both R and R^*. Let $\alpha \in \mathbb{R}$. First, since R is a FIO associated to the local canonical graph C, (A.6), by (A.13)

$$\mathrm{WF}^{\alpha+1/2}(Rf) \subset (C^t) \circ \mathrm{WF}^{\alpha}(f)\,.$$

Since R^*R is an elliptic pseudodifferential operator of order -1,

$$\mathrm{WF}^{\alpha}(f) = \mathrm{WF}^{\alpha+1}(R^*Rf)$$

[**77**, Proposition 6.10, p. 70]. Applying (A.13) to R^* and then to R we see

$$\mathrm{WF}^{\alpha}(f) = \mathrm{WF}^{\alpha+1}(R^*Rf) \subset C \circ \mathrm{WF}^{\alpha+1/2}(Rf) \subset C \circ C^t \mathrm{WF}^{\alpha}(f) = \mathrm{WF}^{\alpha}(f)\,.$$

Here we have used that $C \circ C^t = \mathrm{Id}$ because of the Bolker assumption: p_Y is an injective immersion. This proves

$$\mathrm{WF}^{\alpha}(f) = C \circ \mathrm{WF}^{\alpha+1/2}(Rf)\,. \tag{A.14}$$

If you trace back (A.14) using the expression for C, you get (2.19). Then, the covector $(\theta_0, s_0; a\boldsymbol{\eta_0})$ in (2.19) determines $(x_0, a\theta_0\mathbf{dx})$ by the Bolker assumption. Note that (A.14) is an equality, so other wavefront directions (those not conormal to $L(\varphi_0, s_0)$ or not over points on $L(\varphi_0, s_0)$) will not be visible. □

REMARK A.4. Note that two points in $T^*([0, 2\pi] \times \mathbb{R})$ correspond to $(x_0, a\theta_0)$ in (2.19). We will show they are caused by the ambiguity in parametrization of lines, (2.4). They are the $T^*([0, 2\pi] \times \mathbb{R})$ coordinates of the two points in C that include $(x_0, a\theta_0\mathbf{dx})$:

$$\begin{aligned}
&(x_0, \varphi_0, s_0; a(\theta_0\mathbf{dx} + \mathbf{ds} - (x_0 \cdot \theta_0^\perp)\mathbf{d}\varphi)) \quad \text{and} \\
&(x_0, \varphi_0 + \pi, -s_0; (-a)(\theta(\varphi_0 + \pi)\mathbf{dx} + \mathbf{ds} - (x_0 \cdot \theta^\perp(\varphi_0 + \pi))\mathbf{d}\varphi)) \\
&= (x_0, \varphi_0 + \pi, -s_0; (-a)(-\theta_0\mathbf{dx} + \mathbf{ds} + (x_0 \cdot \theta_0^\perp\mathbf{d}\varphi)))\,.
\end{aligned}$$

These points in T^*Y are $(\varphi_0, s_0; a\mathbf{ds} - a(x_0 \cdot \theta_0^\perp)\mathbf{d}\varphi)$ and $(\varphi_0 + \pi, -s_0; -a\mathbf{ds} - a(x_0 \cdot \theta_0^\perp)\mathbf{d}\varphi)$ and they are mapped into each other under the map in (2.4), $(\varphi, s) \mapsto (\varphi + \pi, -s)$, since $\mathbf{d}\varphi$ stays the same under translation $\varphi \mapsto \varphi + \pi$ and $\mathbf{ds}$ changes to $-\mathbf{ds}$ under the reflection $p \mapsto -p$. Since the Radon transform is invariant under

(2.4), Rf either has wavefront at both points or at neither point, so there is no ambiguity and (2.19) is valid in both directions.

References

[1] M. D. Altschuler, *Reconstruction of the global-scale three-dimensional solar corona*, Topics in Applied Physics, vol. 32, pp. 105–145, Springer-Verlag, New York/Berlin, 1979.

[2] R.H.T. Bates and R.M. Lewitt, *Image reconstruction from projections: I: General theoretical considerations, II: Projection completion methods (theory), III: Projection completion methods (computational examples)*, Optik **50** (1978), I: 19–33, II: 189–204, III: 269–278.

[3] Gregory Beylkin, *The inversion problem and applications of the generalized Radon transform*, Comm. Pure Appl. Math. **37** (1984), 579–599.

[4] Jan Boman and Eric Todd Quinto, *Support theorems for real analytic Radon transforms on line complexes in* $\mathbb{R}^3$, Trans. Amer. Math. Soc. **335** (1993), 877–890.

[5] E.J. Candès and D. L. Donoho, *Curvelets and Reconstruction of Images from Noisy Radon Data*, Wavelet Applications in Signal and Image Processing VIII (M. A. Unser A. Aldroubi, A. F. Laine, ed.), vol. Proc. SPIE 4119, 2000.

[6] Emmanuel Candès and Laurent Demanet, *Curvelets and Fourier Integral Operators*, C. R. Math. Acad. Sci. Paris. Serie I **336** (2003), no. 5, 395–398.

[7] Allan M. Cormack, *Representation of a function by its line integrals with some radiological application*, J. Appl. Physics **34** (1963), 2722–2727.

[8] ———, *Representation of a function by its line integrals with some radiological applications II*, J. Appl. Physics **35** (1964), 2908–2913.

[9] M.E. Davison, *The ill-conditioned nature of the limited angle tomography problem*, SIAM J. Appl. Math. **43** (1983), 428–448.

[10] J. DeStefano and T. Olsen, *Wavelet localization of the Radon transform in even dimensions*, IEEE Trans. Signal Proc. **42** (1994), 2055–2067.

[11] Charles L. Epstein, *Introduction to the Mathematics of Medical Imaging*, Prentice Hall, Upper Saddle River, NJ, USA, 2003.

[12] Adel Faridani, *Tomography and Sampling Theory*, The Radon Transform and Applications to Inverse Problems (Providence, RI, USA), AMS Proceedings of Symposia in Applied Mathematics, American Mathematical Society, 2006.

[13] Adel Faridani, David Finch, E. L. Ritman, and Kennan T. Smith, *Local tomography, II*, SIAM J. Appl. Math. **57** (1997), 1095–1127.

[14] Adel Faridani and E. L. Ritman, *High-resolution computed tomography from efficient sampling*, Inverse Problems **16** (2000), 635–650.

[15] Adel Faridani, E. L. Ritman, and Kennan T. Smith, *Local tomography*, SIAM J. Appl. Math. **52** (1992), 459–484.

[16] David Victor Finch, Ih-Ren Lan, and Gunther Uhlmann, *Microlocal Analysis of the Restricted X-ray Transform with Sources on a Curve*, Inside Out, Inverse Problems and Applications (Gunther Uhlmann, ed.), MSRI Publications, vol. 47, Cambridge University Press, 2003, pp. 193–218.

[17] Joachim Frank, *Three-dimensional electron microscopy of macromolecular assemblies*, Academic Press, San Diego, 1996.

[18] Israel M. Gelfand, M. I. Graev, and N. Ya. Vilenkin, *Generalized Functions*, vol. 5, Academic Press, New York, 1966.

[19] A. B. Goncharov, *Integral geometry and three-dimensional reconstruction of randomly oriented identical particles from their electron microphotos*, Acta Applicandae Mathematicae **11** (1988), 199–211.

[20] Allan Greenleaf and Gunther Uhlmann, *Non-local inversion formulas for the X-ray transform*, Duke Math. J. **58** (1989), 205–240.

[21] ———, *Microlocal techniques in integral geometry*, Contemporary Math. **113** (1990), 121–136.

[22] Victor Guillemin, *Some remarks on integral geometry*, Tech. report, MIT, 1975.

[23] ———, *On some results of Gelfand in integral geometry*, Proceedings Symposia Pure Math. **43** (1985), 149–155.

[24] Victor Guillemin and Shlomo Sternberg, *Geometric Asymptotics*, American Mathematical Society, Providence, RI, 1977.

[25] Marjorie G. Hahn and Eric Todd Quinto, *Distances between measures from 1-dimensional projections as implied by continuity of the inverse Radon transform*, Zeitschrift Wahrscheinlichkeit **70** (1985), 361–380.
[26] Sigurdur Helgason, *The Radon transform on Euclidean spaces, compact two-point homogeneous spaces and Grassman manifolds*, Acta Math. **113** (1965), 153–180.
[27] ———, *The Radon Transform, Second Edition*, Birkhäuser, Boston, 1999.
[28] W. Hoppe and R. Hegerl, *Three-dimensional structure determination by electron microscopy*, Computer Processing of Electron Microscope Images, Springer Verlag, New York, 1980.
[29] Lars Hörmander, *Fourier Integral Operators, I*, Acta Mathematica **127** (1971), 79–183.
[30] ———, *The Analysis of Linear Partial Differential Operators*, vol. I, Springer Verlag, New York, 1983.
[31] V. Isakov, *Inverse Problems for Partial Differential Equations*, Applied Mathematical Sciences, vol. 127, Springer-Verlag, New York, 1998.
[32] Avinash C. Kak and Malcolm Slaney, *Principles of Computerized Tomographic Imaging*, Classics in Applied Mathematics, vol. 33, SIAM, Philadelphia, PA, 2001.
[33] Alexander I. Katsevich, *Cone beam local tomography*, SIAM J. Appl. Math. **59** (1999), 2224–2246.
[34] Alexander I. Katsevich and Alexander G. Ramm, *A method for finding discontinuities from the tomographic data*, Lectures in Appl. Math. **30** (1994), 105–114.
[35] ———, *Pseudolocal tomography*, SIAM J. Appl. Math. **56** (1996), 167–191.
[36] Peter Kuchment, *Generalized Transforms of Radon Type and their Applications*, The Radon Transform and Applications to Inverse Problems (Providence, RI, USA), AMS Proceedings of Symposia in Applied Mathematics, American Mathematical Society, 2006.
[37] Peter Kuchment, Kirk Lancaster, and Ludmilla Mogilevskaya, *On local tomography*, Inverse Problems **11** (1995), 571–589.
[38] Peter Kuchment and Eric Todd Quinto, *Some problems of integral geometry arising in tomography*, The Universality of the Radon Transform, by Leon Ehrenpreis, Oxford University Press, London, 2003.
[39] I.-R. Lan, *On an operator associated to a restricted x-ray transform*, Ph.D. thesis, Oregon State University, 2000.
[40] Serguei Lissianoi, *On stability estimates in the exterior problem for the Radon transform*, Lecture Notes in Appl. Math., vol. 30, pp. 143–147, Amer. Math. Soc., Providence, RI, USA, 1994.
[41] Alfred K. Louis, *Analytische Methoden in der Computer Tomographie*, Universität Münster, 1981, Habilitationsschrift.
[42] ———, *Ghosts in tomography, the null space of the Radon transform*, Mathematical Methods in the Applied Sciences **3** (1981), 1–10.
[43] ———, *Incomplete data problems in X-ray computerized tomography I. Singular value decomposition of the limited angle transform*, Numerische Mathematik **48** (1986), 251–262.
[44] ———, *Development of Algorithms in CT*, The Radon Transform and Applications to Inverse Problems (Providence, RI, USA) (Gestur Olafsson and Eric Todd Quinto, eds.), AMS Proceedings of Symposia in Applied Mathematics, American Mathematical Society, 2006.
[45] Alfred K. Louis and Peter Maaß, *Contour reconstruction in 3-D X-Ray CT*, IEEE Trans. Medical Imaging **12** (1993), no. 4, 764–769.
[46] Alfred K. Louis and Andreas Rieder, *Incomplete data problems in X-ray computerized tomography II. Truncated projections and region-of-interest tomography*, Numerische Mathematik **56** (1986), 371–383.
[47] Peter Maaß, *3D Röntgentomographie: Ein Auswahlkriterium für Abtastkurven*, Zeitschrift für angewandte Mathematik und Mechanik **68** (1988), T 498–T499.
[48] ———, *The interior Radon transform*, SIAM J. Appl. Math. **52** (1992), 710–724.
[49] Wolodymir R. Madych and Stewart A. Nelson, *Polynomial based algorithms for computed tomography*, SIAM J. Appl. Math. **43** (1983), 157–185.
[50] W.R. Madych, *Tomography, approximate reconstruction, and continuous wavelet transforms*, Appl. Comput. Harmon. Anal. **7** (1999), no. 1, 54–100.
[51] Frank Natterer, *Efficient implementation of 'optimal' algorithms in computerized tomography*, Math. Methods in the Appl. Sciences **2** (1980), 545–555.
[52] ———, *The mathematics of computerized tomography*, Classics in Mathematics, Society for Industrial and Applied Mathematics, New York, 2001.

[53] Frank Natterer and Frank Wübbeling, *Mathematical Methods in image Reconstruction*, Monographs on Mathematical Modeling and Computation, Society for Industrial and Applied Mathematics, New York, 2001.

[54] Clifford J. Nolan and Margaret Cheney, *Synthetic Aperture inversion*, Inverse Problems **18** (2002), no. 1, 221–235.

[55] ———, *Microlocal Analysis of Synthetic Aperture Radar Imaging*, Journal of Fourier Analysis and Applications **10** (2004), 133–148.

[56] Ozan Öktem, *Mathematical problems related to the research at CMB and SIDEC Technologies AB*, Tech. report, SIDEC Technologies, AB, Stockholm, 2001.

[57] Victor Palamodov, *Nonlinear artifacts in tomography*, Soviet Physics Doklady **31** (1986), 888–890.

[58] ———, *Reconstruction from Limited Data of Arc Means*, J. Fourier Analysis and Applications **6** (2000), 26–42.

[59] ———, *Reconstructive Integral Geometry*, Monographs in Mathematics, Birkhauser, Boston, MA, USA, 2004.

[60] R. M. Perry, *On reconstructing a function on the exterior of a disc from its Radon transform*, J. Math. Anal. Appl. **59** (1977), 324–341.

[61] Bent Petersen, *Introduction to the Fourier Transform and Pseudo-Differential Operators*, Pittman, Boston, 1983.

[62] Eric Todd Quinto, *The dependence of the generalized Radon transform on defining measures*, Trans. Amer. Math. Soc. **257** (1980), 331–346.

[63] ———, *Tomographic reconstructions from incomplete data–numerical inversion of the exterior Radon transform*, Inverse Problems **4** (1988), 867–876.

[64] ———, *Computed tomography and rockets*, Mathematical Methods in Tomography, Lecture Notes in Mathematics, vol. 1497, Springer Verlag, 1990, pp. 261–268.

[65] ———, *Limited data tomography in non-destructive evaluation*, IMA Volumes in Mathematics and its Applications, vol. 23, pp. 347–354, Springer-Verlag, 1990.

[66] ———, *Singularities of the X-ray transform and limited data tomography in* $\mathbb{R}^2$ *and* $\mathbb{R}^3$, SIAM J. Math. Anal. **24** (1993), 1215–1225.

[67] ———, *Exterior and Limited Angle Tomography in Non-destructive Evaluation*, Inverse Problems **14** (1998), 339–353.

[68] ———, *Local Algorithms in Exterior Tomography*, Journal of Computational and Applied Mathematics (2005), to appear.

[69] Johann Radon, *Über die Bestimmung von Funktionen durch ihre Integralwerte langs gewisser Mannigfaltigkeiten*, Ber. Verh. Sach. Akad. **69** (1917), 262–277.

[70] G.N. Ramachandran and A.V. Lakshminarayanan, *Three dimensional reconstruction from radiographs and electron micrographs: applications of convolutions instead of Fourier Transforms*, Proc. Natl. Acad. Sci. USA **68** (1971), 262–277.

[71] Alexander G. Ramm and Alexander I. Zaslavsky, *Singularities of the Radon transform*, Bull. Amer. Math. Soc. **25** (1993), 109–115.

[72] F. Rashid-Farrokhi, K.J.R. Liu, Carlos A. Berenstein, and David Walnut, *Wavelet-based multiresolution local tomography*, IEEE Trans. Image Processing **6** (1997), 1412–1430.

[73] Lawrence A. Shepp and J. B. Kruskal, *Computerized Tomography: The new medical X-ray technology*, Amer. Mathematical Monthly **85** (1978), 420–439.

[74] Lawrence A. Shepp and S. Srivastava, *Computed tomography of PKM and AKM exit cones*, A. T & T. Technical J. **65** (1986), 78–88.

[75] Kennan T. Smith, Donald C. Solmon, and Solomon L. Wagner, *Practical and mathematical aspects of the problem of reconstructing objects from radiographs*, Bull. Amer. Math. Soc. **83** (1977), 1227–1270.

[76] O. J. Tretiak, *Attenuated and exponential Radon transforms*, Proceedings Symposia Appl. Math. **27** (1982), 25–34.

[77] F. Treves, *Introduction to Pseudodifferential and Fourier integral operators, Volumes 1 & 2*, Plenum Press, New York, 1980.

[78] E.I. Vainberg, I. A. Kazak, and V. P. Kurozaev, *Reconstruction of the internal three-dimensional structure of objects based on real-time integral projections*, Soviet Journal of Nondestructive Testing **17** (1981), 415–423.

Department of Mathematics, Tufts University, Medford, MA 02155, USA
E-mail address: Todd.Quinto@tufts.edu *Web Site:* http://www.tufts.edu/∼equinto